Universiteit
Leiden
The Netherlands

Activity-based protein profiling in drug-discovery

Esbroeck, A.C.M. van

Citation
Esbroeck, A. C. M. van. (2019, May 28). *Activity-based protein profiling in drug-discovery*. Retrieved from https://hdl.handle.net/1887/74006

Version:	Not Applicable (or Unknown)
License:	Leiden University Non-exclusive license
Downloaded from:	https://hdl.handle.net/1887/74006

Note: To cite this publication please use the final published version (if applicable).

Cover Page

Universiteit Leiden

The following handle holds various files of this Leiden University dissertation:
http://hdl.handle.net/1887/74006

Author: Esbroeck, A.C.M. van
Title: Activity-based protein profiling in drug-discovery
Issue Date: 2019-05-28

3

Applications of activity-based protein profiling in developing zebrafish

A.C.M. van Esbroeck
A.F. Stevens
V. Kantae
L.T. Lelieveld
E.J. van Rooden
B.I. Florea
R.C. van Wijk
A.C. Harms
P.H. van der Graaf
J.M.F.G. Aerts
T. Hankemeier
H.S. Overkleeft
M. van der Stelt

ABSTRACT | The zebrafish (*Danio rerio*) is increasingly used as a pre-clinical vertebrate model in drug discovery and development. Here, an activity-based protein profiling (ABPP) method for broad-spectrum profiling of serine hydrolases and kinases in zebrafish larvae is presented. ABPP coupled to mass spectrometry analysis enabled the identification and mapping of 45 hydrolases and 51 kinases throughout early zebrafish development (0-5 days post fertilization), showing a variety of activity profiles. As an application, fatty acid amide hydrolase (FAAH) inhibitor PF04457845 was used in a competitive ABPP setup. FAAH2a was the only inhibited hydrolase among the hydrolases detected by chemical proteomics and downstream inhibition effects were confirmed by lipidomics analysis. With the increasing popularity of zebrafish as a vertebrate animal model and their use in phenotypic drug discovery, the combined approach of comparative and competitive ABPP may serve as a valuable tool in the drug discovery process, complementary to existing methods.

Manuscript in preparation

Introduction

The zebrafish (*Danio rerio*) is a popular model system for embryonic development[1,2] and is increasingly used as a pre-clinical vertebrate model in drug discovery[3,4]. The zebrafish is evolutionary more distinct from humans than rodents are. Nonetheless, 71% of all human proteins and 82% of all disease-causing proteins have zebrafish orthologues[5]. Pharmacological effects of compounds are often conserved, as active sites or ligand binding domains tend to be more homologous[3]. A variety of genetic modification strategies in zebrafish has facilitated the generation of disease models, closely mimicking human diseases. Combined with several other advantages, including small size, rapid development, optical transparency and cost-effective use, the zebrafish is considered an attractive model organism, which is complementary to existing rodent models[6]. Its use has paved the way to whole-animal (semi-)high-throughput screening in phenotypic target discovery and toxicological screening[6–8]. However, target identification and target engagement studies remain challenging. Most biochemical zebrafish studies, especially in embryonic development, rely on protein[9,10] and gene expression[11,12] profiles. Despite the fact that gene and protein expression do not directly translate to protein activity, the activity profile is often not taken into account and the enzymatic state of a protein is not considered.

Activity-based protein profiling (ABPP) may aid in gaining a more complete view on the early development of the zebrafish and may help establish its validity as a model organism in the drug discovery process. ABPP uses active-site directed probes to assess the functional state of an entire enzyme class in a complex protein sample. Fluorescent reporter tags enable rapid sample analysis by sodium dodecyl sulfate polyacrylamide gel electrophoresis (SDS-PAGE) and in-gel fluorescence scanning, whereas affinity tags can be used for target enrichment and subsequent identification by mass spectrometry (MS)[13,14]. The method can be used for inhibitor profiling in a competitive setup. It enables target engagement studies and provides information on the selectivity profile of small molecule modulators within the investigated protein class[15,16]. Alternatively, a comparative setup can be used to map the activity landscape of different biological samples or states[17], e.g. different stages of development, which may enable discovery of biological markers and drug targets[15].

Two important protein classes, the serine hydrolases and kinases, can be targeted by activity-based probes. The serine hydrolases represent approximately 1% of all proteins in mammals and are characterized by a well conserved GXSXG amino acid motif and are involved in a broad spectrum of physiological processes, including signaling and metabolism[14]. Their active-site serine can interact covalently with fluorophosphonate (FP)-based and β-lactone-based probes, such as FP-rhodamine (FP-TAMRA)[14,15] and MB064[18,19]. The kinases, a large protein family with over 500 members, are known for their pivotal roles in cell signaling processes, differentiation, proliferation, and disease[20,21]. A conserved lysine in the kinase active-site offers a reactive group for kinase-targeting probes such as XO44[22]. This probe contains an alkyne moiety which

serves as a ligation handle to introduce a reporter group via a copper(I)-catalyzed azide-alkyne cycloaddition ("click" chemistry)[23]. Serine hydrolases and kinases have been demonstrated as drug targets by successful development of inhibitors and their therapeutic use in various diseases, including cancer , inflammation and Alzheimer's[24,25]. For example, PF04457845, a fatty acid amide hydrolase inhibitor (FAAH), has entered clinical trials for the treatment of neurological disorders[26,27] and kinase inhibitors such as Imatinib and Dasatinib are powerful drugs in cancer treatment[28].

In this study, a comparative ABPP assay was developed to map the serine hydrolase and kinase activity landscape during early zebrafish development (0-5 days post fertilization (dpf)). The assay was subsequently used in a competitive ABPP setup, using PF04457845 as a model drug. PF04457845 targets FAAH[27,29], a membrane-bound serine hydrolase that degrades the endocannabinoid anandamide (AEA) and related amidated lipids[30–33]. Treatment of zebrafish larvae with PF04457845 enabled rapid mapping of the *in vivo* inhibitor interaction profile in a similar fashion as was reported for *in vitro* and *in situ* model systems[16].

Results & Discussion

Comparative ABPP: Mapping zebrafish development

ABPP has previously been used to map the serine hydrolase landscape e.g. in mouse tissue[17]. Here, an ABPP assay was developed to facilitate the use of zebrafish larvae. It was anticipated that the number of proteins expressed would increase over the course of development. Therefore, clear lysate, membrane, and cytosol fractions were prepared from a large batch of 5 dpf larvae and fractions were analyzed by gel-based ABPP using hydrolase probes MB064 and FP-TAMRA (Figure 1A). Extensive labeling was observed, but band overlap impeded band identification by competitive ABPP (data not shown). Chemical proteomics with their biotinylated counterparts, MB108 and FP-biotin respectively, resulted in the identification of 61 different hydrolases (Figure 1B, Supplementary Table S1), of which 46, 33, and 48 were found in the lysate, cytosol, and membrane fractions respectively. Targets were identified as those having ≥ 2-fold enrichment as compared to heat-inactivated controls and a peptide count ≥ 2 with at least 1 unique peptide. In addition, targets were filtered against a putative probe-target list developed for human/mouse-based experiments[34] and zebrafish gene homologues were included. Several of the enriched targets contained a serine hydrolase motif (GXSXG)[35], but were not part of the putative hydrolase target list. These hydrolases are indicated as additional zebrafish targets (Supplementary Table S1).

Several members of the α,β-hydrolase domain containing protein (ABHD) family were detected, as well as a variety of carboxylic ester hydrolases (CEL, CES), and members of the endocannabinoid metabolic pathways such as monoacylglycerol lipase (MGLL) and the fatty acid amide hydrolases (FAAH, FAAH2a, FAAH2b). Of note, even though whole-animal proteomic analysis provides a rapid general overview of the

activity profile, poorly abundant proteins or tissue-specific activities may be lost in the proteomic analysis.

To increase sample throughput and improve experimental ease, the profiling process was streamlined by reducing sample size and simplifying sample preparation. Whole lysates were prepared from samples containing a varying number of larvae per replicate. Inconsistent labeling was observed in the gel-based assay when a single larva was used, whereas using 5 larvae was sufficient to obtain a reproducible labeling pattern between biological replicates (data not shown). The optimized assay conditions were employed in a comparative ABPP setup and enabled assessment of the hydrolase activity landscape throughout development. Larvae were obtained immediately after fertilization at 1, 2, 3, 4 or 5 dpf (5 larvae/replicate). Gel-based analysis of whole lysates labeled with MB064 and FP-TAMRA revealed that both the number of hydrolases and the activity of most hydrolases increased over time (Figure 2). Similarly, coomassie staining showed an overall increase in the number of proteins from 1 dpf onwards. Vitellogenin, one of the main constituents of the yolk sac, was observed as two thick bands at 70 and 120 kDa that decreased over time, in accordance with the use of the yolk as nutrient source[1].

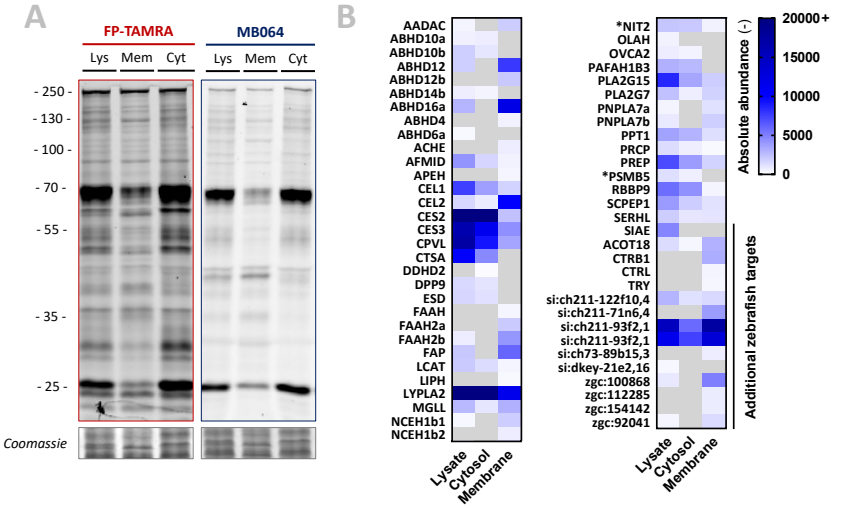

Figure 1 | The serine hydrolase activity profile in zebrafish larvae (5 dpf). Clear lysate (lys), membrane (mem) and cytosol (cyt) fractions from zebrafish larvae (5 dpf) were analyzed by gel-based ABPP and chemical proteomics. (**A**) Proteins were labeled with MB064 (2 µM) or FP-TAMRA (500 nM) (20 min, 28 °C) and 10 µg protein was resolved by SDS-PAGE. Coomassie served as a protein loading control. (**B**) Samples (200 µg protein) were labeled with FP-Biotin and MB108 (10 µM each, 30 min, 28 °C) and analyzed by chemical proteomics. Absolute abundance is summarized in a heat map (blue scale), proteins that were not detected are depicted in grey (n=3). Targets with a non-serine nucleophile are indicated with *, additional zebrafish targets contain a GXSXG motif but were not included in the putative hydrolase target list.

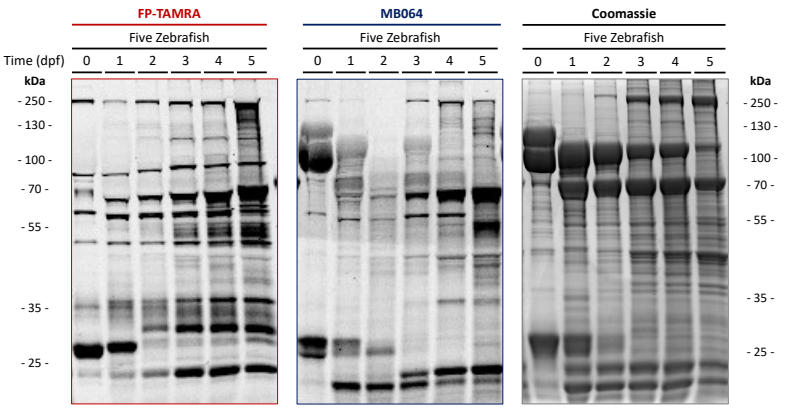

Figure 2 | Comparative ABPP analysis of serine hydrolases during embryonic development. Whole lysate of zebrafish larvae from different development stages (0-5 dpf, 5 larvae/sample) was labeled with FP-TAMRA (500 nM) or MB064 (2 µM) (20 min, 28 °C) and resolved by SDS-PAGE. Coomassie served as a protein loading control.

Next, chemical proteomics was used to identify the hydrolase targets. Whole lysates (5 larvae/replicate, 0-5 dpf) were labeled with probes MB108 and FP-biotin and analyzed by LC-MS after affinity purification and trypsin-digestion (Figure 3A, Supplementary Figure S1, Supplementary Table S1). In total, 45 hydrolases were identified. In line with the gel-based data, the number of hydrolases detected increased over time, as well as their activity.

The activity of several hydrolases coincided with development of the organs in which they are generally highly expressed. For example, a rapid increase in carboxylic esterase 2 and 3 (CES2, CES3) and arylacetamide deacetylase (AADAC) abundance was observed from day 3 on (Figure 3). *ces2*, *ces3* and *aadac* are generally highly expressed in the liver[36,37], of which the growth phase (> 2 dpf)[38] coincides with the increase in CES and AADAC activity as observed by ABPP. Similarly, activity of the pancreatic enzymes chymotrypsin (zgc:92041)[36,37] and carboxylic ester hydrolase 1 and 2 (CEL.1, CEL.2) [36,37] appeared at the end of pancreatic development (> 3 dpf)[39].

Several other hydrolases (including acylaminoacyl-peptide hydrolase (APEH), S-formylgluthatione hydrolase (ESD), OVCA2 esterase (OVCA2) and platelet-activating factor acetylhydrolase isoform 1b gamma subunit (PAFAH1b3) had a more constant activity. Their reported (gene) expression is more uniform across different tissue types[36,37], thus making their activity profiles less sensitive to development of a specific tissue type.

FAAH2b showed the most outstanding activity profile, as it was the only hydrolase which had a reduction in activity during development. FAAH2b is one of the metabolic enzymes in the endocannabinoid system. This system is responsible for the physiological effects of cannabis and is involved in a number of biological processes. In an mRNA-based study, *faah2b* expression was detected directly after fertilization, followed by a

rapid reduction and recovery at 4-5 dpf[40]. High FAAH2b activity levels during fertilization may be required for the hydrolysis of the endocannabinoid AEA and other *N*-acylethanolamines (NAEs). Functional cannabinoid receptors present in the sperm can be activated upon AEA release from female follicle fluids or eggs, thereby hampering fertilization[41,42]. Therefore, rapid degradation of AEA may be beneficial in the fertilization process.

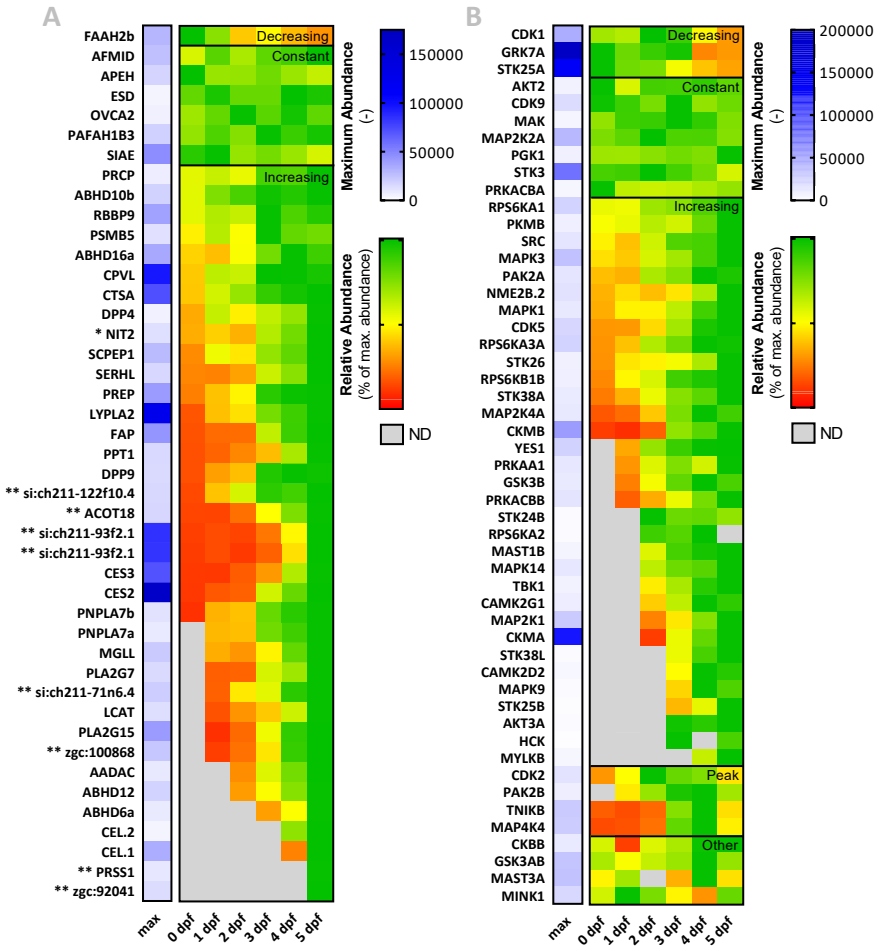

Figure 3 | Serine hydrolase and kinase activity landscape during zebrafish development (0-5 dpf). Heatmap summary of activity-based proteomics of (serine) hydrolases (**A**) and kinases (**B**). (**A**) Zebrafish whole lysates from different development stages (0-5 dpf, 5 larvae/sample) were treated with MB108 and FP-Biotin (10 µM each, 30 min, 28 °C), followed by chemical proteomics analysis. * Indicates targets with a non-serine nucleophile, ** indicates additional zebrafish targets containing a GXSXG motif, which were not included in the putative hydrolase target list. (**B**) Zebrafish whole lysates from different development stages (0-5 dpf, 5 larvae/sample) were treated with XO44 (10 µM, 60 min, 28 °C) and conjugated to biotin-azide (40 µM, 60 min, 28 °C), followed by chemical proteomics analysis. (**A**-**B**) Data is represented as absolute abundance at the time point with maximum abundance (blue scale) (individual data points in Supplementary Figure S1-2). Relative abundance is expressed as a percentage of maximum abundance per protein (green-red scale) or as not detected (grey) (mean, n=6). Outliers as determined by ROUT's outlier test (5%) have been excluded from calculations.

Several other endocannabinoid metabolic enzymes were also detected including the 2-arachidonoyl glycerol (2-AG) hydrolytic enzymes MGLL, ABHD12 and ABHD6a, starting at 1, 2 and 3 dpf, respectively, and increased over time. A similar increase in mRNA expression has been observed for *abhd6a*[43]. In contradiction with the chemical proteomics data, *mgll* expression peaked at 8 hpf, but was stably expressed from 1 dpf onward, while *abhd12* expression decreased from 2 dpf onwards in the same study[43]. Thus, gene expression and protein activity are not always directly correlated.

The ABPP assay was extended with kinase targeting probe XO44[22], which interacts with a well-conserved reactive lysine in the kinase active site (Figure 3B, Supplementary Figure S2, Supplementary Table S2). Lysates were incubated with the probe, which was subsequently conjugated to a biotin reporter to enable enrichment and proteomic analysis. In total, 51 kinases were identified, having ≥ 2-fold enrichment as compared to vehicle-treated controls, a peptide count ≥ 2 and at least 1 unique peptide. In addition, targets (or their human orthologues) had to be annotated as kinases in the Uniprot protein database. Of note, in contrast to the hydrolase probes, XO44 labels available kinase active-sites dependent on their affinity, but not necessarily on their active state.

The number of detected kinases increased throughout development and in general their abundance increased time dependently. For example, cyclin dependent kinase 5 (CDK5), serine/threonine kinase 38a (STK38A) and mitogen-activated protein kinase 1 and 3 (MAPK1, MAPK3) abundance steadily increased over time from fertilization onward. However, also different labeling profiles were observed. STK25B and MAPK14, for example, were detected at later stages and increased from there on, while STK24B remained stable once expressed. In contrast, STK25A decreased time dependently from 0 dpf onwards and CDK1 was stably expressed until 3 dpf and subsequently reduced.

A more distinct labeling profile was observed for p21 protein (CDC42/rac)-activated kinase 2b (PAK2b) and CDK2 which peaked at 3-4 dpf and 2 dpf respectively. Brain-subtype creatine kinase (CKBB) was abundant after fertilization, followed by a strong decrease at 1 dpf and a subsequent recovery and increase. These profiles suggest tight regulation of activity throughout the embryonic phase and may be related to important developmental processes. In human embryonic stem cells CDK2 plays a crucial role in balancing cell proliferation and cell death. Its downregulation induces a loss of pluripotency as well as differentiation toward extraembryonic lineages[44]. The function of PAK2b, or its human homologue PAK2, in development has not yet been described.

Several kinases also showed a steady abundance over time, which may indicate a more general role or a less tight regulation. For example, the metabolic kinase phosphoglycerate kinase (PGK), an ATP-generating enzyme in the glycolytic pathway[45], is present at a very constant level, which corresponds with its house-keeping character. Similarly, v-akt murine thymoma viral oncogene homolog 2 (AKT2) is stably active from day 1 onward. CRISPR/Cas9 mediated disruption of *akt2* expression has been shown to

cause developmental deficits and increase lethality in zebrafish larvae, thereby stressing its importance throughout development[46].

Competitive ABPP: PF04457845 profiling

Having established the activity profile of serine hydrolases, a competitive ABPP assay was developed to enable rapid *in vivo* target engagement assessment and off-target profiling. Zebrafish larvae (5 dpf) were exposed to vehicle (DMSO, 0.1%) or FAAH inhibitor PF04457845 (1 µM, 8 h) in their swimming medium. The bioavailability of the inhibitor was assessed by measuring the drug concentration in the blood using LC-MS analysis. PF04457845 was detected at a concentration of 0.5 µM (n=1), thereby validating internal drug exposure in the treated larvae. After treatment, lysates were analyzed by gel-based ABPP using fluorescent probes MB064 and FP-TAMRA (Figure 4A-B) or chemical proteomics using their biotinylated counterparts MB108 and FP-biotin respectively (Figure 4C). PF04457845 inhibited fatty acid amide hydrolase 2a (FAAH2a), a FAAH analogue, without affecting the other 58 detected hydrolases. This is in line with human *in vitro* and *in situ* studies in which PF04457845 only targeted FAAH and FAAH2[16]. Of note, PF04457845's intended target FAAH falls below the detection limit in whole lysate fractions and inhibition could thus not be determined.

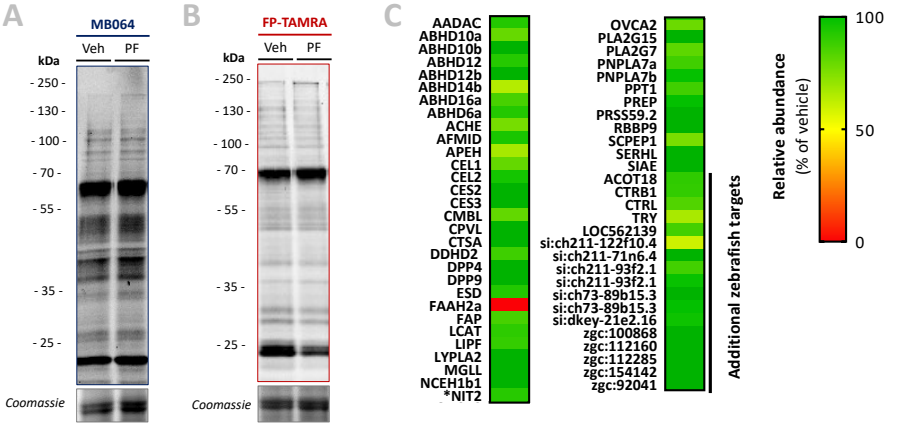

Figure 4 | Competitive ABPP of zebrafish larvae *in vivo* treated with FAAH-inhibitor PF04457845. (**A**-**B**) Gel-based activity profiling of zebrafish larvae (5 dpf) treated *in vivo* with vehicle or PF04457845 (1 µM, 8 h, 28 °C). Clear lysate was labeled with (**A**) MB064 (1 µM) or (**B**) FP-TAMRA (500 nM) (20 min, 28 °C) and 12.5 µg protein was resolved by SDS-PAGE. Coomassie is shown as a loading control. (**C**) Heatmap summary of chemical proteomics analysis of zebrafish larvae (5 dpf, 300 µg protein) treated *in vivo* with vehicle or PF04457845 (1 µM, 8 h, 28 °C) with probes MB108 and FP-biotin (10 µM each, 30 min, 28 °C). Data is expressed relative to vehicle treated (mean, n=4). Targets with a non-serine nucleophile are indicated with *, additional zebrafish targets contain a GXSXG motif but were not included in the putative hydrolase target list.

FAAH[30,32] and FAAH2a[47,48] both hydrolyze the endocannabinoid AEA[49] as well as other *N*-acylethanolamines (NAEs). To assess the functional effect of PF04457845 on FAAH(2), endocannabinoid levels were investigated by LC-MS (Figure 5A). The larvae were exposed to the drug in their swimming medium (1 µM PF04457845, 2-24 h). The

levels of FAAH substrate AEA increased after 2 hours of treatment and reached a steady state after 5 hours, thus indicating that PF04457845 uptake was sufficient to inhibit FAAH/FAAH2 *in vivo.* The levels of a second endocannabinoid 2-AG were not affected by the drug (Figure 5A). Semi-targeted lipidomics was performed to assess the effects of PF04457845 on the overall lipid profile. In total, 223 lipids from 15 different lipid classes were detected in 5 dpf zebrafish larvae (Figure 5B). PF04457845 exposure (8 h) increased NAE levels, while other lipid classes remained unchanged. These data correspond with the clean interaction profile of PF04457845 as determined by ABPP.

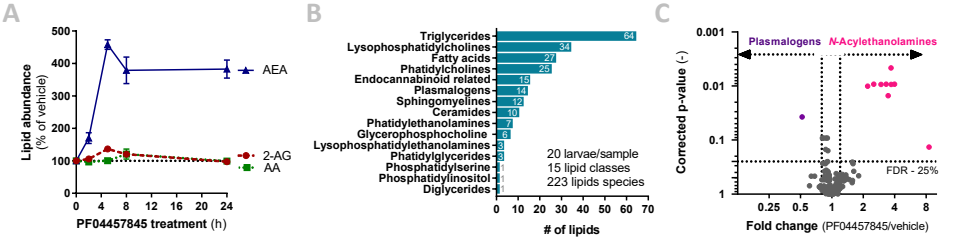

Figure 5 |Lipidomics analysis of zebrafish larvae *in vivo* treated with FAAH inhibitor PF04457845. (**A**) Time response curve of endocannabinoids (AEA, 2-AG) and metabolite arachidonic acid (AA). Zebrafish larvae (5 dpf) were treated *in vivo* with vehicle or PF04457845 (1 µM, 2-24 h). Endocannabinoid levels were measured by LC-MS and expressed relative to vehicle-treated controls at the corresponding time point (mean ± SEM, n=3). (**B-C**) Zebrafish larvae (5 dpf) were treated with vehicle or PF04457845 (1 µM, 8 h) and lipid levels were analyzed by LC-MS. (**B**) Total number of lipid species detected in zebrafish larvae sorted by lipid class. (**C**) Volcano plot summary of lipidomics data. Lipids with a fold change (FC) threshold of ≥ 1.20 or ≤ 0.80 and Benjamini-Hochberg false discovery rate (FDR) ≤ 25%, circles colored by lipid class (mean fold change, n=3).

Conclusion

In summary, a proteomics-based ABPP method was developed and enabled rapid mapping of the activity landscape of two large protein families in zebrafish larvae. Over 50 serine hydrolases were targeted using broad-spectrum probes FP-biotin and MB108, as well as 51 kinases using the reactive-lysine targeting probe XO44. This enabled mapping of the hydrolase activity and kinase landscape throughout early zebrafish development (0-5 dpf). In addition, FAAH inhibitor PF04457845 was used to showcase zebrafish larvae as a simple *in vivo* model for drug discovery.

Phenotypic (semi-high throughput) drug screening is gaining popularity as it enables discovery of therapeutic drugs, even without having a validated drug-target[4,50]. The comparative chemical proteomics workflow may aid the discovery of potential serine hydrolase or kinase drug targets by enabling activity profile assessment between observed phenotypes. The competitive setup extends the assay, as it enables target identification and off-target screening. In addition, the comparative assay serves as a complementary tool to study developmental processes at the protein activity level, circumventing current limitations such as poor antibody availability for zebrafish proteins and limited translatability of mRNA levels to protein expression and activity.

Experimental procedures

Materials, probes and inhibitors

Fluorophosphonate-TAMRA (FP-TAMRA) and MB064, were synthesized in house as previously described[18,51]. XO44 was synthesized according to literature procedures[22]. All synthesized compounds were at least 95% pure and were analyzed by LC-MS, NMR, and HRMS. Stocks are prepared in DMSO. Other chemicals were purchased from Sigma Aldrich, unless indicated otherwise.

Zebrafish sample collection

Zebrafish husbandry

Wildtype zebrafish were housed at Leiden University, the Netherlands in compliance with the local animal welfare regulations and were maintained according to standard protocols (zfin.org). Embryos were collected from family crosses of AB/TL wild-type strain (license number 10612, Leiden University) and were grown at 28.5 °C in embryo medium (60 µg/mL Instant Ocean sea salts (Sera Marin), methylene blue) in the dark. All experiments were performed using zebrafish embryos and larvae before the feeding stage, as specified by the EU animal protection Directive 2010/63/EU.

Sample collection development stages

Fertilized embryos were transferred to a petri dish in embryo medium and were maintained at 28.5 °C in the dark until 5 dpf. At 0, 1, 2, 3, 4, or 5 dpf embryos/larvae were collected. Emrbyos/larvae were washed three times with embryo medium. For each replicate, five embryos/larvae were transferred to a 1.5 mL Eppendorf tube using a Pasteur pipet. Alternatively, a large number of zebrafish larvae (> 100) was washed and transferred to a 1.5 mL Eppendorf tube. In either case, excess liquid was removed and the embryos/larvae were flash frozen in liquid nitrogen and stored at -80 °C until further use.

PF04457845 in vivo *treatment*

Embryos were raised in an incubator at 28.5 °C. At 5 dpf, larvae were treated with vehicle (0.05% DMSO) or PF04457845 (1 µM, 2-24 h, as indicated). For lipid extraction, three replicates of 20 larvae each were collected, washed three times with 80/20 embryo medium/methanol (v/v). For ABPP four replicates of ~60 larvae each were collected, without additional washing. Excess liquid was removed and the larvae were flash frozen in liquid nitrogen and stored at -80 °C until further use.

Activity-based protein profiling

Sample preparation

Zebrafish larvae were thawed on ice and homogenized in a sufficient amount of sucrose lysis buffer (250 mM sucrose, 20 mM HEPES pH 7.2, 2 mM DTT, 1 mM $MgCl_2$, 2 U/mL benzonase) or kinase lysis buffer (100 mM HEPES pH 8.0, 1.5 mM $MgCl_2$, 1 mM EGTA pH 8.0, 150 mM NaCl, 1 mM Na_3VO_4, 0.1% (v/v) NP-40, 10 mM NaF, 1x mammalian protease inhibitor (M250, Amresco), 2 U/mL benzonase) with a pestle motor (whole lysate). Clear lysate was obtained as the supernatant fraction after two low-speed centrifugation steps (5 min, 1000 *g*, 4 °C) in which the cell debris was removed. Clear lysate was separated into cytosol and membrane fractions by ultracentrifugation (30,000 *g*, 60-90 min, 4 °C). The membrane pellet was resuspended in sucrose or kinase lysis buffer. Protein concentration of clear lysate, membrane, and cytosol fractions was determined by Bradford assay and samples were diluted (1-2 mg/mL) in their according buffers. Samples were flash frozen in liquid nitrogen and stored at -80 °C until further use.

For time-course experiments, the larvae (five per replicate) were homogenized in 100 µL sucrose or kinase lysis buffer using a pestle motor. The entire sample (± 100 µL whole lysate) was used for proteomics experiments. For the gel-based assay, 20 µL lysate was used per activity-based probe.

Gel-based ABPP

Protein samples were incubated with activity-based probes MB064 (2 µM) or FP-TAMRA (500 nM). The reaction was quenched with Laemmli buffer (15 min, 50 °C) and samples were resolved by SDS-PAGE (10% acrylamide gel, ± 80 min, 180 V) along with protein marker (PageRuler™ Plus, Thermo Fisher). In-gel fluorescence was measured in the Cy3- and Cy5-channel (ChemiDoc™ MP, Bio-Rad) and gels were stained with Coomassie after scanning. Fluorescence was quantified and normalized to Coomassie staining using ImageLab™ software (Bio-Rad).

Label-free proteomics

The label-free chemical proteomics workflow was modified from Van Rooden *et al.*[34]. For serine hydrolase activity profiling, the lysates were incubated with serine hydrolase probe cocktail (10 µM MB108, 10 µM FP-biotin, 30 min, 28 °C, 300 rpm) and as a negative control a denatured protein sample (1% SDS, 5 min, 100 °C) was taken along. For kinase profiling, the lysates were incubated with kinase-probe XO44 (10 µM, 30 min, 28 °C, 300 rpm). Treatment with vehicle (2% DMSO) was taken along as a negative control. Subsequently, the probe was conjugated to biotin-azide by addition of click mix (final concentration: 1 mM $CuSO_4 \cdot (H_2O)_5$, 0.56 mM sodium ascorbate, 0.2 mM THPTA, 40 µM biotin-azide) and subsequent incubation (60 min, 28 °C, 300 rpm).

Precipitation, alkylation and avidin enrichment were performed according to protocol[34]. Avidin beads were washed twice with SDS/PBS, followed by three PBS washes. On-bead digestion was performed overnight according to protocol and after sample preparation the dried peptides were stored at -20 °C until LC-MS analysis. Prior to measurement, samples were reconstituted in 40 µL LC-MS sample solution and transferred to LC-MS vials. LC-MS data was analyzed by ProteinLynx Global SERVER™ (PLGS, Waters) and IsoQuant software[52] (www.proteomeumb.org/MZw.html) (settings: minimal peptide score 5.5/6.0, false discovery rate 1%). Excel was used for further analysis, with the following cut-offs: unique peptides ≥ 1, identified peptides ≥ 2, ratio positive over negative control ≥ 2, part of hydrolase target list and/or containing a GXSXG serine hydrolase motif (additional zebrafish targets) (probe cocktail), or having the annotation kinase in the Uniprot database (XO44). Graphs were created using GraphPad Prism 7 (GraphPad).

Lipidomics analysis: Endocannabinoids

Lipid extraction

Endocannabinoids and their congeners were quantified using LC-MS/MS analysis. The lipid extraction was performed on ice. In brief, 20 zebrafish larvae at 5 dpf were transferred to 1.5 mL Eppendorf tubes, spiked with deuterated internal standard mix for endocannabinoids (*N*-arachidonoylethanolamine (AEA)-d8, *N*-arachidonoyldopamine (NADA)-d8, *N*-docosahexaenoyl-ethanolamide (DHEA)-d4, 2-arachidonoylglycerol (2-AG)-d8, *N*-stearoylethanolamine (SEA)-d3, *N*-palmitoylethanolamine (PEA)-d4, *N*-linoleoylethanolamine (LEA)-d3 and *N*-oleoylethanolamine (OEA)-d4), followed by the addition of ammonium acetate buffer (100 µL, 0.1 M, pH 4). After extraction with methyl *tert*-butyl ether (800 µL), the tubes were thoroughly sonicated until the sample was homogenous. The samples were mixed for 6 min using a bullet blender at medium speed (Next Advance Inc.), followed by a centrifugation step (5,000 *g*, 12 min, 4 °C). Then 750 µL of the upper methyl *tert*-butyl ether layer was transferred into a clean 1.5 mL Eppendorf tube. Samples were dried in a speed-vac (Eppendorf) followed by reconstitution in acetonitrile/H_2O (30 µL, 90/10, v/v). The reconstituted samples were centrifuged (14,000 *g*, 3 min, 4 °C) before transferring into LC-MS vials. 5 µL of sample was injected for LC-MS analysis.

LC-MS/MS analysis

A targeted analysis of 21 endocannabinoids and related NAEs was measured using an Acquity UPLC I class Binary solvent manager pump (Waters) in conjugation with AB SCIEX 6500 quadrupole-ion trap (QTRAP) (AB Sciex). Separation was performed with an Acquity HSS T3 column (1.2 x 100 mm, 1.8 µm) maintained at 45 °C. The aqueous mobile phase A consisted of 2 mM ammonium formate and 10 mM formic acid, and the organic mobile phase B was acetonitrile. The flow rate was set to 0.4 mL/min; initial gradient conditions were 55% B held for 2 min and linearly ramped to 100% B over 6 min and held for 2 min; after 10 s, the system returned to initial conditions and held 2 min before next injection. Electrospray ionization-MS was operated in positive mode for measurement of 21 endocannabinoids and NAEs, and a selective Multiple Reaction Mode (sMRM) was used for quantification. Peak area integration was performed with MultiQuant (AB Sciex, Version 3.0.2) data analysis software. The obtained peak areas of targets were corrected by appropriate internal standards. Calculated response ratios, determined as the peak area ratios of the target analytes to the respective internal standards, were used to obtain absolute concentrations from their respective calibration curves.

Table 1 | Target list of endocannabinoids and *N*-acylethanolamines and their validation parameters. The method is validated in terms of linearity sensitivity (LOQ), process efficiency (matrix effect with recovery) and precision. Endogenous concentrations are expressed as mean ± SEM.

Abbreviation	Metabolite name	Process efficiency (%)	Correlation coefficient (R^2)	Precision (% RSD)	Lipid level (fmol/larvae)
2&1AG (20:4)	Arachidonoylglycerol	78	0.998	5	2270 ± 59
AEA (20:4)	Anandamide	85	0.999	12	0.5 ± 0.02
DHEA (22:6)	*N*-Docosahexaenoyl ethanolamide	49	0.999	4	42 ± 1.6
LEA (18:2)	*N*-Linoleoylethanolamide	79	0.999	3	0.38 ± 0.11
OEA (18:1)	*N*-Oleoylethanolamide	84	0.999	6	1.2 ± 0.28
PEA (16:0)	*N*-Palmitoylethanolamide	87	0.999	3	21.6 ± 0.9
SEA (18:0)	*N*-Stearoylethanolamide	91	0.999	2	11.7 ± 0.6
DEA (22:4)	*N*-Docosatetraenoyl ethanolamide	48	0.998	19	0.4 ± 0.02
DGLEA (18:3)	Dihomo-γ-Linolenoyl ethanolamide	65	0.999	35	0.1 ± 0.01
2-LG (18:2)	2-Linoleoyl glycerol	63	0.999	8	6153 ± 493
1-LG (18:2)	1-Linoleoyl glycerol	74	0.981	7	773 ± 66
2-OG (18:1)	2-Oleoyl glycerol	73	0.999	3	17999 ± 1740
1-OG (18:1)	1-Oleoyl glycerol	N/A	0.986	3	2564 ± 191
EPEA (20:5)	*N*-Eicosapentaenoyl ethanolamide	65	0.999	5	7.3 ± 0.44
POEA (16:1)	*N*-Palmitoleoylethanolamide	99	0.999	4	0.8 ± 0.04
PDEA (15:0)	*N*-Pentadecanoylethanolamide	82	0.999	7	0.2 ± 0.01
AA (20:4)	Arachidonic Acid	122	0.998	7	80167 ± 5530

Lipidomics analysis: Targeted lipidomics

Sample extraction

The endocannabinoid extraction protocol was followed, with the following adjustment. In addition to the endocannabinoid internal standards, non-endogenous lipid internal standards were added (lysophosphatidylcholine (LPC) 17:0, phosphatidylethanolamine (PE) 17:0/17:0, phosphatidylcholine (PC) 17:0/17:0, sphingomyelin (SM) d18:1/17:0, triglyceride (TG) 17:0/17:0/17:0, ceramide (Cer) d18:1/17:0 and fatty acid (FA) 17:0-d33). Each sample was injected on three different lipidomics platforms: endocannabinoids (5 µL), positive lipids (2 µL) and negative lipids (8 µL).

LC-MS/MS analysis

The endocannabinoid analysis was followed as described above. Both lipidomics methods (positive and negative lipids) are adapted and modified from previously published work[16]. In brief, these methods are measured on an Acquity UPLC Binary solvent manager pump (Waters) coupled to a Synapt G2 electrospray ionization quadrupole time-of-flight (ESI-Q-TOF, Waters) high

resolution mass spectrometer using reference mass correction. The chromatographic separation was achieved on an Acquity HSS T3 column (1.2 x 100 mm, 1.8 µm) maintained at 40 °C for both methods. The positive lipid run includes targets from different lipid classes including (lyso)phosphatidylcholines, triglycerides, ceramides. (Lyso)phosphatidylethanolamines and sphingomyelins were separated using a flow of 0.4 mL/min over a 16 min gradient. In positive mode, the mobile phase A consisted of 60/40 (v/v) acetonitrile/H_2O with 10 mM ammonium formate, and the mobile phase B consisted of 10/90 (v/v) acetonitrile/isopropanol with 10 mM ammonium formate. The negative lipids constitute mainly free fatty acids and (lyso)phosphatidylcholines were separated with a flow of 0.4 mL/min over a 15 min gradient. In negative mode, the aqueous mobile phase A consisted of 5/95 (v/v) acetonitrile/H_2O with 10 mM ammonium formate, and the organic mobile phase B consisted of 99% (v/v) methanol with 10 mM ammonium formate. The targets in both lipid methods were detected full scan (100-1000 m/z) in their respective ion charge mode.

PF04457845 quantification

Sample extraction

PF04457845 was quantified using LC-MS/MS analysis in blood samples pooled from 20-25 treated zebrafish larvae at 5 dpf (1 µM PF04457845, 8 h). The blood sample (total ~83 nL) was collected from anatomical locations of the larval circulation using a pulled needle (borosilicate glass capillary, original diameter: 0.5 mm, Sutter Instruments) in a micromanipulator, connected to a manual CellTram pump (Eppendorf) under 20x microscopic magnification (Leica). For determination of sample volume, an image was taken of each sample's blood content within the needle. To prevent coagulation, needles and collection tubes were coated with heparin. The sample extraction was performed on ice. 200 µL of acetonitrile was added to the blood samples. The samples were vortexed and then centrifuged (13,000 *g*, 10 min). 150 µL of supernatant was evaporated to dryness using a speedvac (Eppendorf) and reconstituted in 10 µL of acetonitrile.

LC-MS/MS analysis

PF04457845 was measured using an Acquity UPLC I class Binary solvent manager pump (Waters) in conjugation with AB SCIEX 6500 quadrupole-ion trap (QTRAP) (AB Sciex). Separation was performed with Acquity HSS T3 column (1.2 x 100 mm, 1.8 µm) maintained at 45 °C. The aqueous mobile phase A consisted of 2 mM ammonium formate and 10 mM formic acid, and the organic mobile phase B was acetonitrile. The flow rate was set to 0.5 mL/min; initial gradient conditions were 60% B held for 0.5 min and linearly ramped to 100% B over 2.5 min and held for 0.5 min; after 10 s the system returned to initial conditions and held 1.5 min before next injection. Electrospray ionization-MS was operated in positive mode for measurement of PF04457845 and a selective Multiple Reaction Mode (sMRM) was used for quantification. The ion masses monitored were Q1/Q3 456/335 (m/z). Peak area integration was performed with MultiQuant (AB Sciex, Version 3.0.2) data analysis software. The limit of detection (LOD) was 1 pM and the linear range used was from 1 to 1000 pM.

Statistical methods

All statistical measures and methods are included in the respective Figure or Table captions. In brief, all data are shown as the mean ± SEM where applicable. A Student's *t*-test (unpaired, two-tailed) was used to determine differences between two groups. All statistical analyses were conducted using Excel (Microsoft) or GraphPad Prism 7 (GraphPad), and a p-value < 0.05 was considered significant throughout unless indicated otherwise. For the lipidomics analysis a Benjamini-Hochberg correction was applied to obtain multicomparison corrected p-values and a false discovery rate of 25% was applied.

Supplementary data

Table S1 | Identified hydrolase targets in zebrafish. Abbreviations and descriptions as annotated on uniprot.org. * Indicates targets with a GXSXG-domain that are not annotated, their molecular function is based on gene ontology.

Protein	Description	Protein	Description
AADAC	Arylacetamide deacetylase	**MGLL**	Monoglyceride lipase
ABHD10a	α-β hydrolase domain containing 10a	**NCEH1B,1**	Neutral cholesterol ester hydrolase 1b, tandem duplicate 1
ABHD10b	α-β hydrolase domain containing 10b	**NCEH1B,2**	Neutral cholesterol ester hydrolase 1b, tandem duplicate 2
ABHD12 *si:ch211-117n7.7i*	α-β hydrolase domain containing 12	**NIT2**	Omega-amidase NIT2
ABHD14b	α-β hydrolase domain containing 14b	**OLAH**	Oleoyl-ACP hydrolase
ABHD16a	α-β hydrolase domain containing 16a	**OVCA2**	Esterase OVCA2
ABHD4	α-β hydrolase domain containing 4	**PAFAH1B3**	Platelet-activating factor acetylhydrolase isoform 1b γ subunit
ABHD6a	α-β hydrolase domain containing 6a	**PLA2G15**	Phospholipase A2 group XV
ACHE	Acetylcholinesterase	**PLA2G7**	Platelet-activating factor acetylhydrolase
ACOT18	Acyl-CoA thioesterase 18	**PNPLA6**	Patatin-like phospholipase domain-containing 6
AFMID	Kynurenine formamidase	**PNPLA7a**	Patatin-like phospholipase domain-containing 7a
APEH	Acylaminoacyl-peptide hydrolase	**PNPLA7b**	Patatin-like phospholipase domain-containing 7b
CEL,1	Carboxylic ester hydrolase	**PPT1**	Palmitoyl-protein thioesterase 1
CEL,2	Carboxylic ester hydrolase	**PPT2**	Palmitoyl-protein thioesterase 2
CES2	Carboxylic ester hydrolase	**PRCP**	Prolylcarboxypeptidase
CES3	Carboxylic ester hydrolase	**PREP**	Prolyl endopeptidase
CMBL	Carboxymethylenebutenolidase homolog	**PRSS1**	Trypsin
CPVL	Carboxypeptidase - vitellogenic-like	**PRSS59.1**	Protease serine 59 tandem duplicate 1
CTRB1	Chymotrypsinogen B1	**PSMB5**	Proteasome subunit beta type
CTRL	Chymotrypsin-like	**RBBP9**	Retinoblastoma-binding protein 9
CTSA	Cathepsin A	**SCPEP1**	Carboxypeptidase
DPP4	Dipeptidyl-peptidase 4	**SERHL**	Serine hydrolase-like protein
DPP9	Dipeptidyl-peptidase 9	**si:ch211-122f10.4**	* Serine-type carboxypeptidase activity
ESD	S-formylglutathione hydrolase	**si:ch211-71n6.4**	* Carboxylic ester hydrolase activity
FAAH	Fatty acid amide hydrolase	**si:ch211-93f2.1**	* Carboxylic ester hydrolase activity
FAAH2A	Fatty-acid amide hydrolase 2a	**si:ch73-89b15.3**	* Carboxylic ester hydrolase activity
FAAH2B	Fatty-acid amide hydrolase 2b	**si:dkey-21e2.16**	* Serine-type endopeptidase activity
FAP	Fibroblast activation protein α	**SIAE**	Sialic acid acetylesterase
LCAT	Lecithin-cholesterol acyltransferase	**TRY**	Trypsin
LIPF	Lipase member F	**zgc:100868**	* Serine-type endopeptidase activity
LIPH	Lipase member H	**zgc:112160**	* Serine-type endopeptidase activity * Chymotrypsinogen B1 like protein
LOC562139	Chymotrypsinogen B1 like protein	**zgc:112285**	* Serine-type endopeptidase activity
LYPLA1	Lysophospholipase I	**zgc:154142**	* Serine-type endopeptidase activity
LYPLA2	Lysophospholipase II	**zgc:92041**	* Serine-type endopeptidase activity

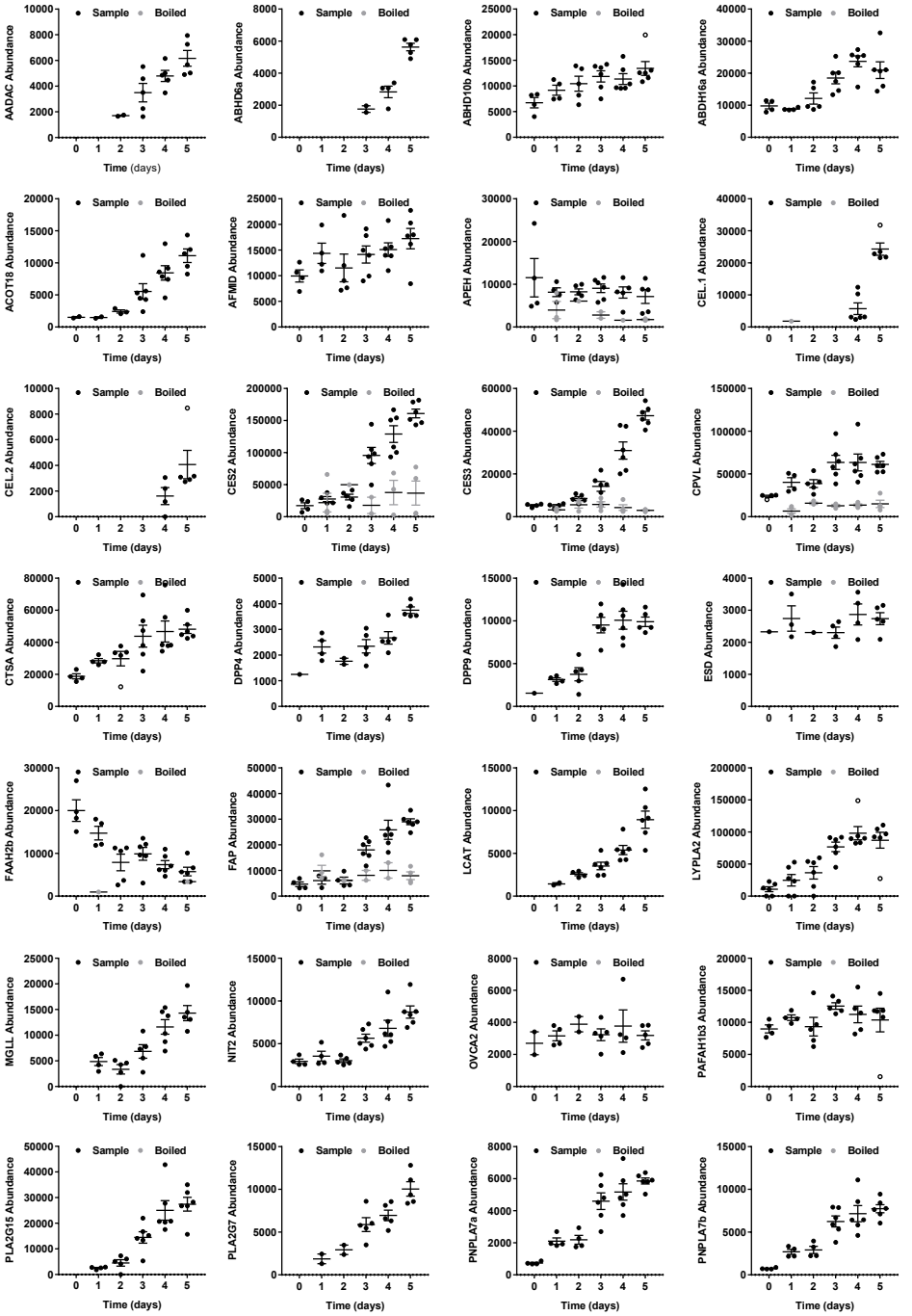

Figure S1 (1/2) | Chemical proteomics analysis of (serine) hydrolases during zebrafish development.

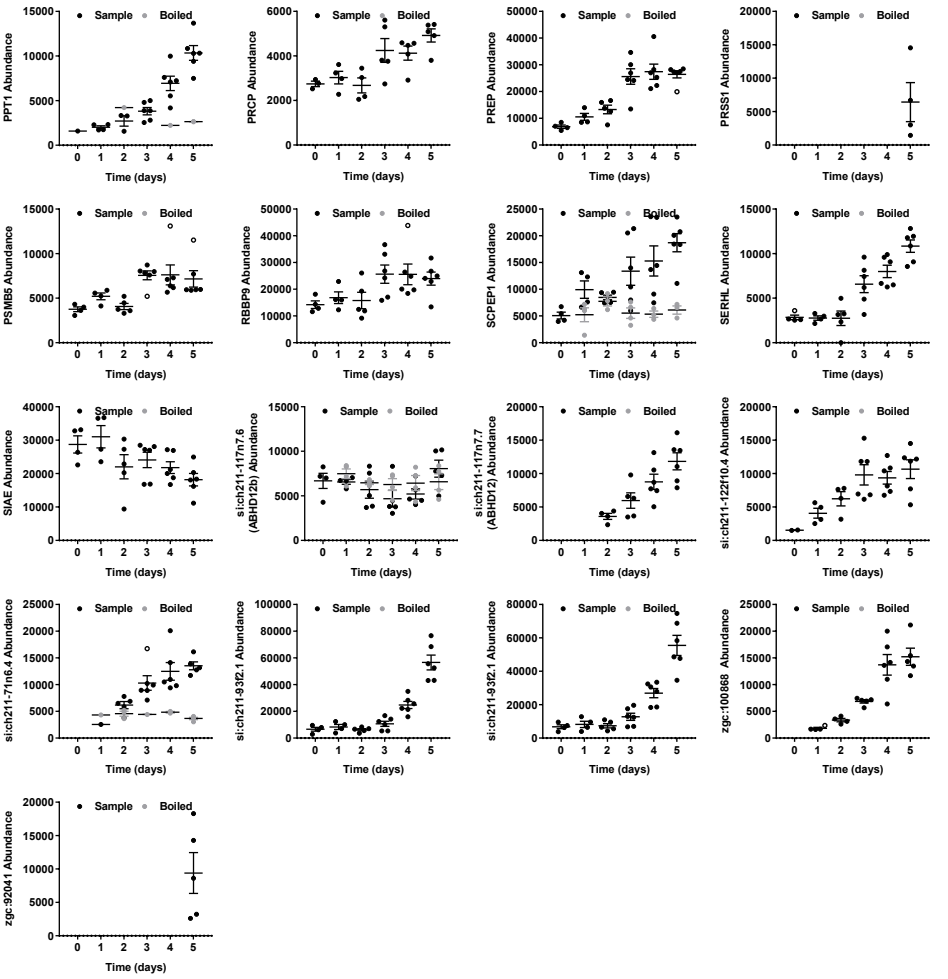

Figure S1 (2/2) | Chemical proteomics analysis of (serine) hydrolases during zebrafish development. Zebrafish whole lysates from different development stages (0-5 dpf, 5 larvae/sample) were treated with MB108 and FP-biotin (10 µM each, 30 min, 28 °C), followed by chemical proteomics analysis. Samples boiled (1% SDS, 5 min, 95 °C) prior to probe incubation served as negative control for each time point. Cut-offs for target selection: ratio positive over negative control ≥ 2, unique peptides ≥ 1, identified peptides ≥ 2 for at least one time point. Targets must be part of hydrolase target list and/or containing a GXSXG serine hydrolase motif. Data is expressed as absolute abundance (mean ± SEM and individual data points) for samples (black fill, n=6) or boiled controls (grey fill, n=4). Outliers as determined with a ROUT outlier test (5%) are depicted with open circles for non-boiled samples only. Undetected proteins in individual samples are not included in plots or calculations.

Table S2 | Identified kinase targets in zebrafish. Abbreviations and descriptions as annotated on uniprot.org.

Protein	Description	Protein	Description
AKT2	v-akt murine thymoma viral oncogene homolog 2	**MINK1**	Misshapen-like kinase 1
AKT3A	v-akt murine thymoma viral oncogene homolog 3a	**MYLKB**	Myosin light chain kinase b
CAMK2D2	Calcium/calmodulin-dependent protein kinase type II delta 2 chain	**NME2B.2**	NME/NM23 nucleoside diphosphate kinase 2b tandem duplicate 2
CAMK2G1	Calcium/calmodulin-dependent protein kinase (CaM kinase) II gamma 1	**PAK2A**	P21 protein (Cdc42/Rac)-activated kinase 2a
CDK1	Cell division control protein 2	**PAK2B**	p21 protein (Cdc42/Rac)-activated kinase 2b
CDK2	Cyclin-dependent kinase 2	**PGK1**	Phosphoglycerate kinase (Fragment)
CDK5	Cyclin-dependent kinase 5	**PKMB**	Pyruvate kinase
CDK9	Cyclin-dependent kinase 9	**PRKAA1**	Non-specific serine/threonine protein kinase
CKBB	Brain-subtype creatine kinase	**PRKACBA**	Protein kinase cAMP-dependent catalytic β a
CKMA	Creatine kinase, muscle a	**PRKACBB**	Protein kinase cAMP-dependent catalytic β b
CKMB	Ckmb protein	**RPS6KA1**	Ribosomal protein S6 kinase
GRK7A	Rhodopsin kinase 1	**RPS6KA2**	Ribosomal protein S6 kinase
GSK3AB	Glycogen synthase kinase 3 alpha b	**RPS6KA3A**	Ribosomal protein S6 kinase
GSK3B	Glycogen synthase kinase 3	**RPS6KB1B**	Ribosomal protein S6 kinase
HCK	Tyrosine-protein kinase	**SRC**	Proto-oncogene tyrosine-protein kinase Src
MAK	Male germ-cell associated kinase	**STK24B**	Serine/threonine kinase 24b
MAP2K1	Mitogen-activated protein kinase kinase 1	**STK25A**	Serine/threonine kinase 25a
MAP2K2A	Mitogen-activated protein kinase kinase 2	**STK25B**	Serine/threonine kinase 25b
MAP2K4A	Mitogen-activated protein kinase kinase 4A	**STK26**	Serine/threonine protein kinase 26
MAP4K4	Mitogen-activated protein kinase kinase kinase kinase 4	**STK3**	Serine/threonine-protein kinase 3
MAPK1	Mitogen-activated protein kinase	**STK38A**	Serine/threonine kinase 38a
MAPK3	Mitogen-activated protein kinase	**STK38L**	Serine/threonine kinase 38-like
MAPK9	Mitogen-activated protein kinase	**TBK1**	TANK-binding kinase 1
MAPK14	Mitogen-activated protein kinase	**TNIKB**	TRAF2 and NCK-interacting kinase b
MAST1B	Microtubule-associated serine/threonine kinase 1b	**YES1**	Tyrosine-protein kinase yes
MAST3A	Microtubule-associated serine/threonine kinase 3a		

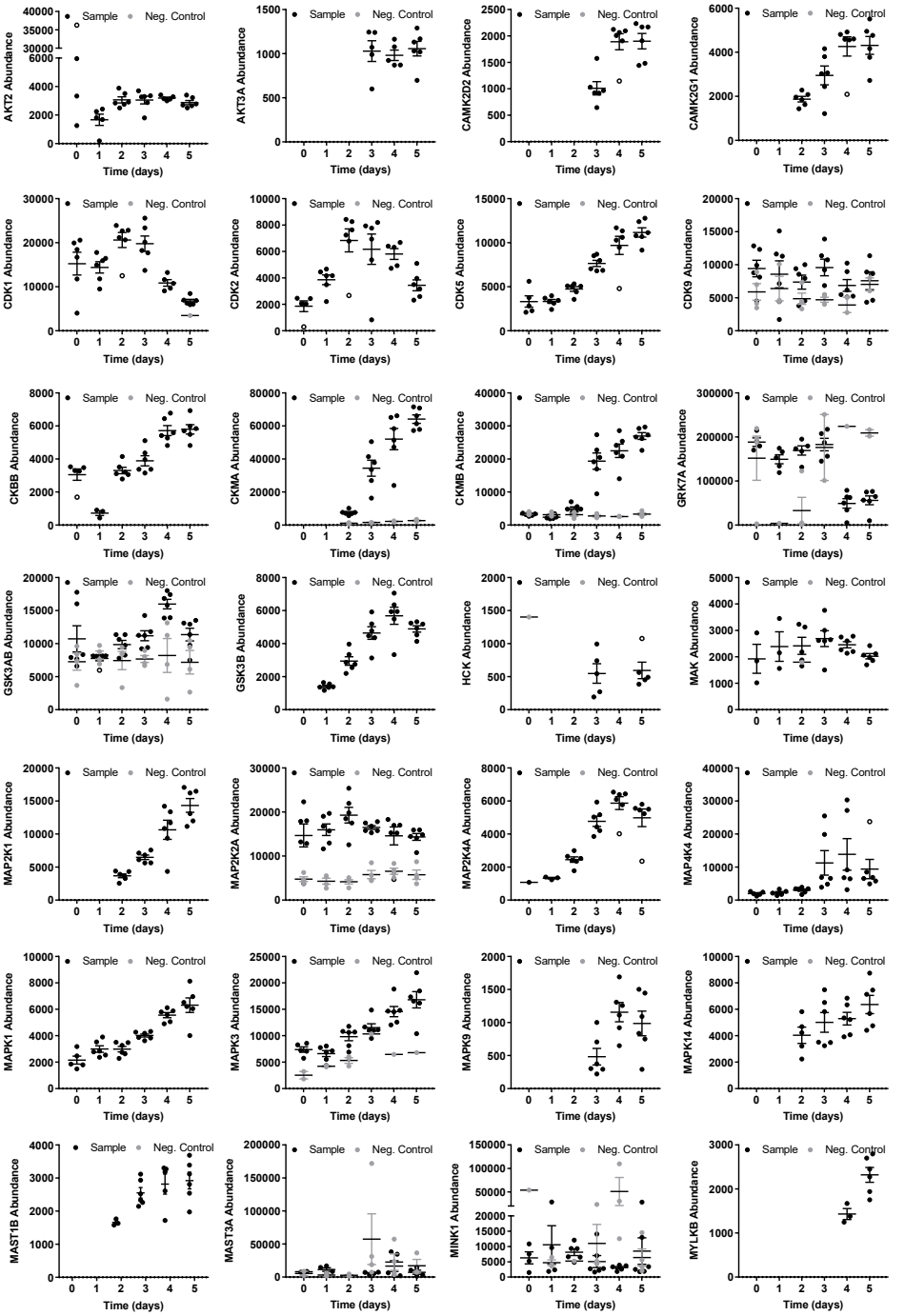

Figure S2 (1/2) | Chemical proteomics analysis of kinases during zebrafish development.

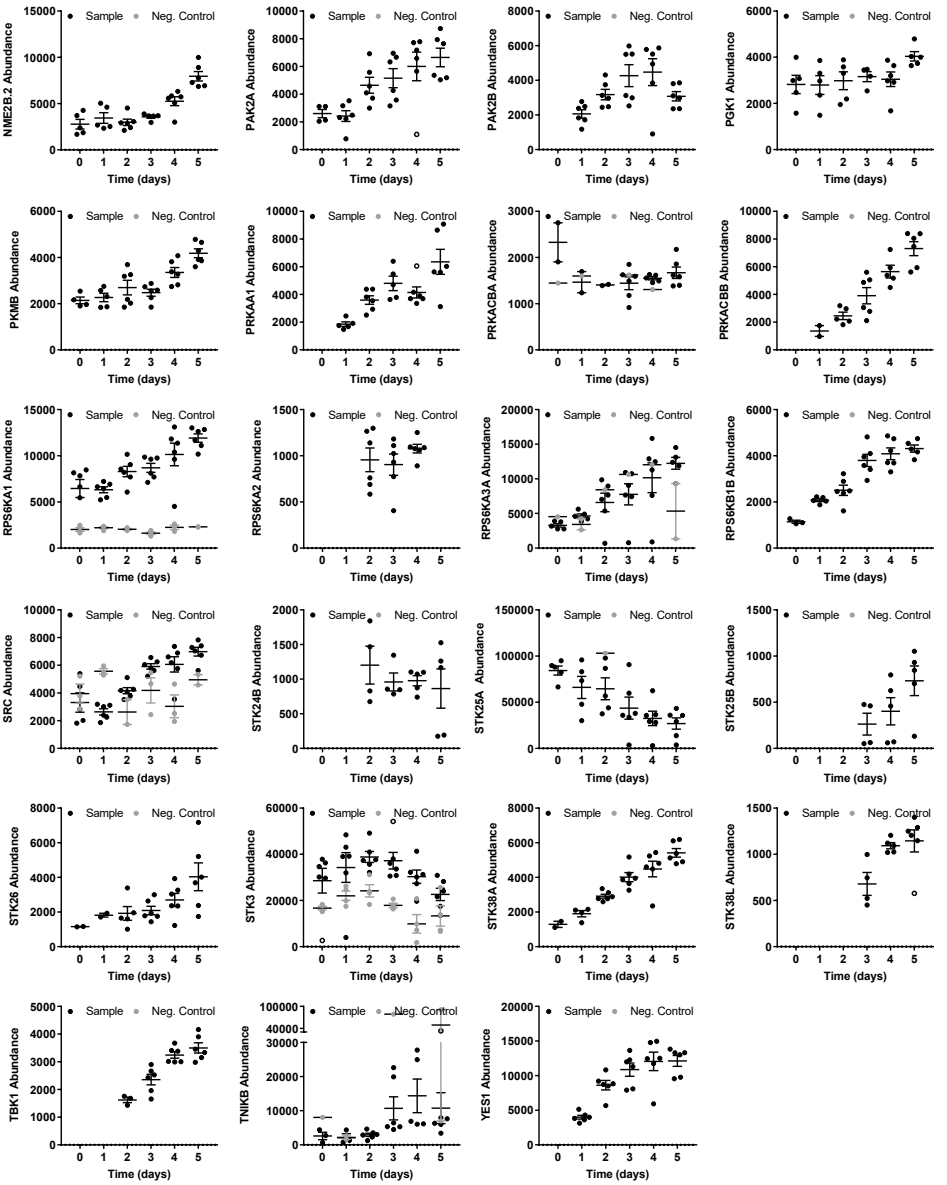

Figure S2 (2/2) | Chemical proteomics analysis of kinases during zebrafish development. Zebrafish whole lysates from different development stages (0-5 dpf, 5 larvae/sample) were treated with XO44 (10 µM, 30 min, 28 °C) and subsequently conjugated to biotin-azide (40 µM, 60 min, 28 °C), followed by chemical proteomics analysis. Vehicle treated sample served as negative control for each time point. Cut-offs for target selection: ratio positive over negative control ≥ 2, unique peptides ≥ 1, identified peptides ≥ 2 for at least one time point. Targets must be annotated as kinase in the Uniprot database. Data is expressed as absolute abundance (mean ± SEM and individual data points) for samples (black fill, n=6) or vehicle treated controls (grey fill, n=4). Outliers as determined with a ROUT outlier test (5%) are depicted as open circles for non-boiled samples only. Undetected proteins in individual samples are not included in plots or calculations.

References

1. Kimmel, C. B., Ballard, W. W., Kimmel, S. R., Ullmann, B. & Schilling, T. F. Stages of embryonic development of the zebrafish. *Dev. Dyn.* **203,** 253–310 (1995).
2. Link, B. A. & Megason, S. G. in *Source Book of Models for Biomedical Research* 103–112 (Humana Press, 2008). ISBN: 9781588299338.
3. MacRae, C. A. & Peterson, R. T. Zebrafish as tools for drug discovery. *Nat. Rev. Drug Discov.* **14,** 721–731 (2015).
4. Rennekamp, A. J. & Peterson, R. T. 15 Years of Zebrafish Chemical Screening. *Curr. Opin. Chem. Biol.* **24,** 58–70 (2015).
5. Howe, K. *et al.* The zebrafish reference genome sequence and its relationship to the human genome. *Nature* **496,** 498–503 (2013).
6. Lieschke, G. J. & Currie, P. D. Animal models of human disease: Zebrafish swim into view. *Nature Reviews Genetics* **8,** 353–367 (2007).
7. Bowman, T. V. & Zon, L. I. Swimming into the future of drug discovery: In vivo chemical screens in zebrafish. *ACS Chem. Biol.* **5,** 159–161 (2010).
8. Zon, L. I. & Peterson, R. T. In vivo drug discovery in the zebrafish. *Nature Reviews Drug Discovery* **4,** 35–44 (2005).
9. Tay, T. L. *et al.* Proteomic analysis of protein profiles during early development of the zebrafish, Danio rerio. *Proteomics* **6,** 3176–3188 (2006).
10. Alli Shaik, A. *et al.* Functional mapping of the zebrafish early embryo proteome and transcriptome. *J. Proteome Res.* **13,** 5536–5550 (2014).
11. Kudoh, T. *et al.* A gene expression screen in zebrafish embryogenesis. *Genome Res.* **11,** 1979–1987 (2001).
12. White, R. J. *et al.* A high-resolution mRNA expression time course of embryonic development in zebrafish. *Elife* **6,** (2017).
13. van Rooden, E. J., Bakker, A. T., Overkleeft, H. S. & van der Stelt, M. Activity-Based Protein Profiling. *eLS* 1–9 (2018).
14. Liu, Y., Patricelli, M. P. & Cravatt, B. F. Activity-based protein profiling: The serine hydrolases. *Proc. Natl. Acad. Sci.* **96,** 14694–14699 (1999).
15. Niphakis, M. J. & Cravatt, B. F. Enzyme Inhibitor Discovery by Activity-Based Protein Profiling. *Annu. Rev. Biochem.* **83,** 341–377 (2014).
16. Van Esbroeck, A. C. M. *et al.* Activity-based protein profiling reveals off-target proteins of the FAAH inhibitor BIA 10-2474. *Science* **356,** 1084–1087 (2017).
17. Baggelaar, M. P. *et al.* Chemical Proteomics Maps Brain Region Specific Activity of Endocannabinoid Hydrolases. *ACS Chem. Biol.* **12,** 852–861 (2017).
18. Baggelaar, M. P. *et al.* Development of an activity-based probe and in silico design reveal highly selective inhibitors for diacylglycerol lipase-α in brain. *Angew. Chemie - Int. Ed.* **52,** 12081–12085 (2013).
19. Baggelaar, M. P. *et al.* Highly Selective, Reversible Inhibitor Identified by Comparative Chemoproteomics Modulates Diacylglycerol Lipase Activity in Neurons. *J. Am. Chem. Soc.* **137,** 8851–8857 (2015).
20. Tarkiainen, T. H. *et al.* Stability over time of short-term heart rate variability. *Clin. Auton. Res.* **15,** 394–399 (2005).
21. Manning, G., Whyte, D. B., Martinez, R., Hunter, T. & Sudarsanam, S. The protein kinase complement of the human genome. *Science* **298,** 1912–34 (2002).
22. Zhao, Q. *et al.* Broad-spectrum kinase profiling in live cells with lysine-targeted sulfonyl fluoride probes. *J. Am. Chem. Soc.* **139,** 680–685 (2017).
23. Rostovtsev, V. V., Green, L. G., Fokin, V. V. & Sharpless, K. B. A stepwise huisgen cycloaddition process: Copper(I)-catalyzed regioselective 'ligation' of azides and terminal alkynes. *Angew. Chemie - Int. Ed.* **41,** 2596–2599 (2002).

24. Bachovchin, D. A. & Cravatt, B. F. The pharmacological landscape and therapeutic potential of serine hydrolases. *Nat. Rev. Drug Discov.* **11,** 52–68 (2012).
25. Klaeger, S. *et al.* The target landscape of clinical kinase drugs. *Science* **358,** eaan4368 (2017).
26. Johnson, D. S. *et al.* Discovery of PF-04457845: A highly potent, orally bioavailable, and selective urea FAAH inhibitor. *ACS Med. Chem. Lett.* **2,** 91–96 (2011).
27. Huggins, J. P., Smart, T. S., Langman, S., Taylor, L. & Young, T. An efficient randomised, placebo-controlled clinical trial with the irreversible fatty acid amide hydrolase-1 inhibitor PF-04457845, which modulates endocannabinoids but fails to induce effective analgesia in patients with pain due to osteoarthritis of th. *Pain* **153,** 1837–1846 (2012).
28. Zhang, J., Yang, P. L. & Gray, N. S. Targeting cancer with small molecule kinase inhibitors. *Nature Reviews Cancer* **9,** 28–39 (2009).
29. Li, G. L. *et al.* Assessment of the pharmacology and tolerability of PF-04457845, an irreversible inhibitor of fatty acid amide hydrolase-1, in healthy subjects. *Br. J. Clin. Pharmacol.* **73,** 706–716 (2012).
30. Cravatt, B. F. *et al.* Molecular characterization of an enzyme that degrades neuromodulatory fatty-acid amides. *Nature* **384,** 83–87 (1996).
31. Kathuria, S. *et al.* Modulation of anxiety through blockade of anandamide hydrolysis. *Nat. Med.* **9,** 76–81 (2003).
32. Devane, W. A. *et al.* Isolation and structure of a brain constituent that binds to the cannabinoid receptor. *Science* **258,** 1946–1949 (1992).
33. Long, J. Z. *et al.* Dual blockade of FAAH and MAGL identifies behavioral processes regulated by endocannabinoid crosstalk in vivo. *Proc. Natl. Acad. Sci. U. S. A.* **106,** 20270–5 (2009).
34. van Rooden, E. J. *et al.* Mapping in vivo target interaction profiles of covalent inhibitors using chemical proteomics with label-free quantification. *Nat. Protoc.* **13,** 752–767 (2018).
35. Long, J. Z. & Cravatt, B. F. The metabolic serine hydrolases and their functions in mammalian physiology and disease. *Chem. Rev.* **111,** 6022–6063 (2011).
36. Wu, C. *et al.* BioGPS: An extensible and customizable portal for querying and organizing gene annotation resources. *Genome Biol.* **10,** 130 (2009).
37. BioGPS - your Gene Portal System. Available at: http://biogps.org/. (Accessed: 1st December 2018)
38. Tao, T. & Peng, J. Liver development in zebrafish (Danio rerio). *Journal of Genetics and Genomics* **36,** 325–334 (2009).
39. Tiso, N., Moro, E. & Argenton, F. Zebrafish pancreas development. *Mol. Cell. Endocrinol.* **312,** 24–30 (2009).
40. Krug, R. G. *et al.* The endocannabinoid gene faah2a modulates stress-associated behavior in zebrafish. *PLoS One* **13,** e0190897 (2018).
41. Schuel, H. *et al.* Cannabinoids inhibit fertilization in sea urchins by reducing the fertilizing capacity of sperm. *Pharmacol. Biochem. Behav.* **40,** 609–615 (1991).
42. Schuel, H. *et al.* N-Acylethanolamines in human reproductive fluids. in *Chemistry and Physics of Lipids* **121,** 211–227 (2002).
43. Oltrabella, F., Melgoza, A., Nguyen, B. & Guo, S. Role of the endocannabinoid system in vertebrates: Emphasis on the zebrafish model. *Dev. Growth Differ.* **59,** 194–210 (2017).
44. Neganova, I., Zhang, X., Atkinson, S. & Lako, M. Expression and functional analysis of G1 to S regulatory components reveals an important role for CDK2 in cell cycle regulation in human embryonic stem cells. *Oncogene* **28,** 20–30 (2009).
45. Watson, H. C. *et al.* Sequence and structure of yeast phosphoglycerate kinase. *EMBO J.* **1,** 1635–1640 (1982).
46. Zhang, D., Wang, J., Zhou, C. & Xiao, W. Zebrafish akt2 is essential for survival, growth, bone development, and glucose homeostasis. *Mech. Dev.* **143,** 42–52 (2017).

47. Wei, B. Q., Mikkelsen, T. S., McKinney, M. K., Lander, E. S. & Cravatt, B. F. A second fatty acid amide hydrolase with variable distribution among placental mammals. *J. Biol. Chem.* **281,** 36569–36578 (2006).
48. McPartland, J. M., Glass, M., Matias, I., Norris, R. W. & Kilpatrick, C. W. A shifted repertoire of endocannabinoid genes in the zebrafish (Danio rerio). *Mol. Genet. Genomics* **277,** 555–570 (2007).
49. Di Marzo, V. Endocannabinoid signaling in the brain: biosynthetic mechanisms in the limelight. *Nat. Neurosci.* **14,** 9–15 (2011).
50. Kithcart, A. & MacRae, C. A. Using Zebrafish for High-Throughput Screening of Novel Cardiovascular Drugs. *JACC Basic to Transl. Sci.* **2,** 1–12 (2017).
51. Janssen, A. P. A. *et al.* Development of a Multiplexed Activity-Based Protein Profiling Assay to Evaluate Activity of Endocannabinoid Hydrolase Inhibitors. *ACS Chem. Biol.* **13,** 2406–2413 (2018).
52. Liao, Z., Wan, Y., Thomas, S. N. & Yang, A. J. IsoQuant: A software tool for stable isotope labeling by amino acids in cell culture-based mass spectrometry quantitation. *Anal. Chem.* **84,** 4535–4543 (2012).